IEEE Photonics Journal
An IEEE Photonics Society Publication

Open Access

Terahertz Waveforms Generated by Second-Order Nonlinear Polarization in GaAs/AlAs Coupled Multilayer Cavities Using Ultrashort Laser Pulses

Volume 5, Number 3, June 2013

Takahiro Kitada, Member, IEEE
Sho Katoh
Toshikazu Takimoto
Yoshinori Nakagawa
Ken Morita
Toshiro Isu

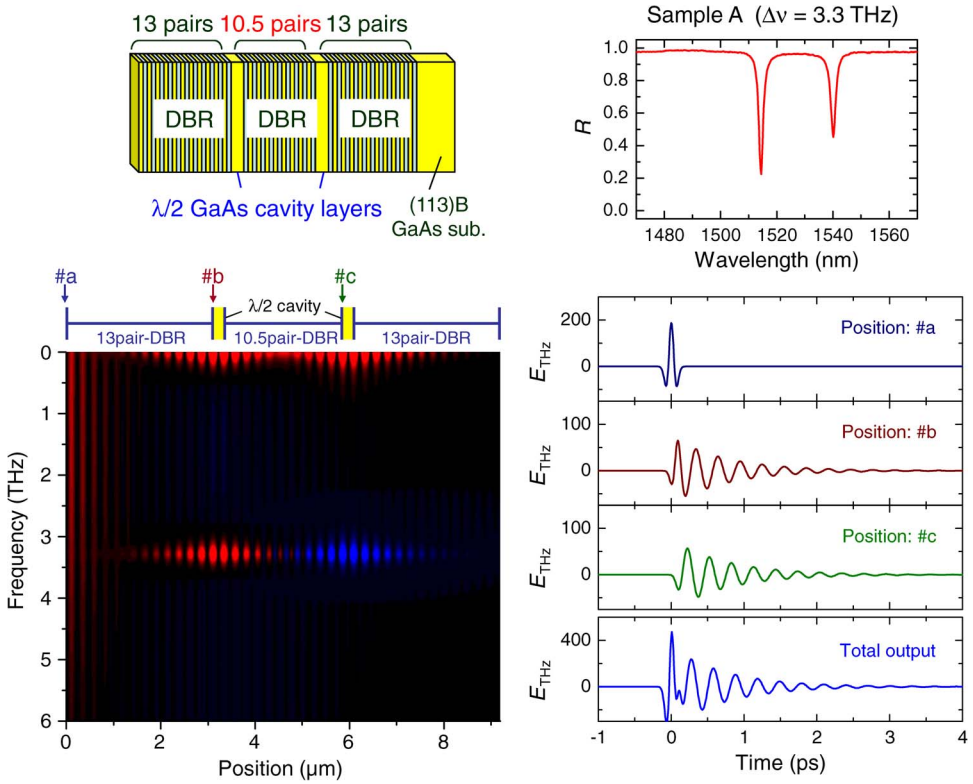

DOI: 10.1109/JPHOT.2013.2267536
1943-0655/$31.00 ©2013 IEEE

Terahertz Waveforms Generated by Second-Order Nonlinear Polarization in GaAs/AlAs Coupled Multilayer Cavities Using Ultrashort Laser Pulses

Takahiro Kitada,[1] *Member, IEEE*, Sho Katoh,[1] Toshikazu Takimoto,[1] Yoshinori Nakagawa,[1,2] Ken Morita,[3] and Toshiro Isu[1]

[1]Center for Frontier Research of Engineering, Institute of Technology and Science, The University of Tokushima, Tokushima, 770-8506, Japan
[2]Nichia Corporation, Anan, 774-8601, Japan
[3]Graduate School of Engineering, Chiba University, Chiba, 263-8522, Japan

DOI: 10.1109/JPHOT.2013.2267536
1943-0655/$31.00 ©2013 IEEE

Manuscript received May 15, 2013; revised May 31, 2013; accepted June 3, 2013. Date of publication June 10, 2013; date of current version June 18, 2013. This work was supported in part by a Grant-in-Aid for Scientific Research (B) under Grant 22360030 from the Japan Society for the Promotion of Science (JSPS). The work of K. Morita was done while he was with the University of Tokushima. Corresponding author: T. Kitada (e-mail: kitada@frc.tokushima-u.ac.jp).

Abstract: Temporal terahertz waveforms generated from GaAs/AlAs coupled multilayer cavity structures were simulated and compared with experimental results. Femtosecond laser pulses covering two cavity-mode frequencies were used for the difference frequency generation (DFG) in the terahertz region. The Fourier components dependent on the frequency and spatial position were determined for the second-order nonlinear polarization induced by a 100-fs Gaussian pulse injection. When the temporal waveform was simulated using the Fourier components, the oscillating behavior due to the efficient DFG of the two cavity modes was clearly observed after the initial ultrafast response near the incident surface. Assuming the exponential decay of signal sensitivity in the high-frequency region, the simulated results were consistent with the experimentally measured ones for coupled cavity structures grown on (113)B GaAs substrates.

Index Terms: Terahertz generation, optical microcavity, III-V semiconductors, frequency mixing, femtosecond laser.

1. Introduction

Useful terahertz sources based on semiconductor materials have been widely investigated because of the wide range of possible applications, which include wireless communications, spectroscopy, and imaging. Many types of devices, such as quantum cascade lasers (QCLs) [1]–[3], resonant tunneling diodes [4], and photomixers [5], [6] have been studied and developed for continuous-wave terahertz emitters. However, although there has been significant progress on terahertz QCLs, near-room-temperature operation has not yet been demonstrated. Efficient wavelength conversion devices based on difference frequency generation (DFG) in III-V semiconductors are attractive for novel emitters that can operate at room temperature due to the large second-order nonlinearity. Efficient terahertz DFG has previously been demonstrated using a GaP crystal excited by two individual lasers [7]–[9]. In addition, femtosecond laser technologies have made it possible to generate terahertz pulses covering extremely broad bandwidths [10]–[12].

We have recently proposed planar-type and room-temperature-operable terahertz emission devices based on the DFG of two cavity modes in a GaAs/AlAs coupled multilayer cavity, in which two half-wavelength $(\lambda/2)$ cavity layers are coupled by an intermediate distributed Bragg reflector (DBR) multilayer [13]. The optical frequency difference between the two modes can be precisely defined in the terahertz region by the number of periods of the coupling DBR multilayer. The internal electric field of each cavity mode is strongly enhanced in both $\lambda/2$ cavity layers, so that strong mixed signals of the two modes can be generated when the coupled cavities are grown on non-(001) GaAs substrates. Note that the growth on the non-(001) substrate is essential because the effective second-order nonlinear coefficient is zero on the (001) orientation due to the crystal symmetry [14], [15]. A strong sum-frequency generation (SFG) signal was obtained from a GaAs/AlAs coupled multilayer cavity grown on a (113)B GaAs substrate by simultaneous excitation of the two cavity modes with 100 fs laser pulses [16]–[18]. The peak intensity of the SFG signal was more than 400 times greater than that of the second-harmonic generation signal from the (113)B GaAs bulk substrate. This indicates that the coupled multilayer cavity structure on the high-index GaAs substrate would act as efficient optical-frequency mixers because of the enhanced electric fields of two cavity modes. In addition, DFG signals from the (113)B coupled cavity samples were also demonstrated at room temperature by time-resolved waveform measurements using 100 fs laser pulses and a photoconductive (PC) antenna [19], [20]. In this work, temporal terahertz waveforms generated by 100 fs Gaussian pulses were simulated for GaAs/AlAs coupled multilayer cavity structures. The internal electric field distributions simulated by the transfer matrix method were used to characterize the terahertz DFG through the second-order nonlinear process. The simulated results were compared with the experimentally measured results for the (113)B coupled cavity samples.

2. Terahertz DFG Simulation

Let us consider the second-order nonlinear polarization induced by a 100 fs Gaussian pulse to understand terahertz DFG in the GaAs/AlAs coupled multilayer cavity. The Fourier component $f_g(\omega)$ of the incident Gaussian pulse is given by

$$f_g(\omega) = \sqrt{2\pi}\tau \exp\left(-\frac{\tau^2(\omega-\omega_0)^2}{2}\right), \tag{1}$$

where ω_0 and $2\tau\sqrt{\ln 2}$ are the central angular frequency and pulse duration defined as full width at half maximum (FWHM), respectively. The electric field of $E(z,t)$ at a certain position z inside the coupled cavity is expressed as

$$E(z,t) = \sum_{\omega} f_g(\omega) A(z,\omega) e^{i\phi(z,\omega)} e^{-i\omega t}, \tag{2}$$

where the modulated amplitude $A(z,\omega)$ and phase $\phi(z,\omega)$ can be determined with conventional transfer matrix methods. According to the second-order nonlinear optical process, the product of $E(z,t)$ and $E^*(z,t)$ gives the nonlinear polarization $P(z,t)$ that contributes to terahertz DFGs, which is given as

$$P(z,t) = \sum_{\omega}\sum_{\omega'} \chi^{(2)}(z,\omega,\omega') f_g(\omega) f_g(\omega') A^*(z,\omega) A(z,\omega') e^{-i\phi(z,\omega)} e^{i\phi(z,\omega')} e^{-i(\omega'-\omega)t}, \tag{3}$$

where $\chi^{(2)}(z,\omega,\omega')$ is the second-order nonlinear susceptibility for the DFG, and the asterisk denotes the complex conjugate. Substituting Ω and $\Delta\omega$ for $\omega'+\omega$ and $\omega'-\omega$, respectively, (3) becomes

$$P(z,t) = \sum_{\Delta\omega} P_{\Delta\omega}(z) e^{-i\Delta\omega t}, \tag{4}$$

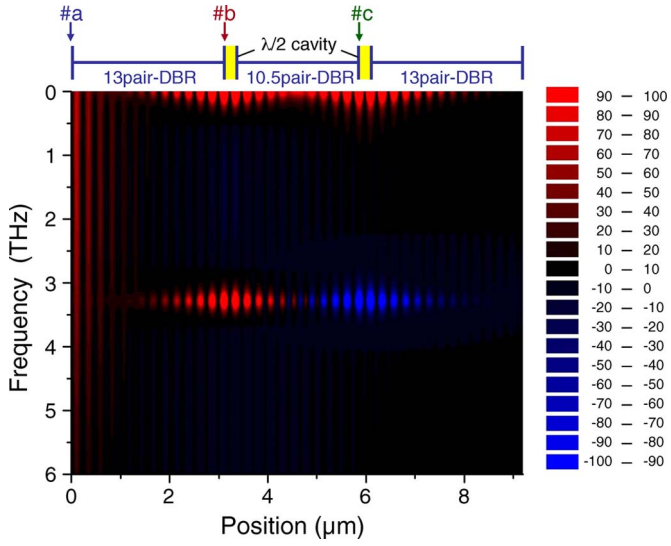

Fig. 1. Position-dependent spectral map of $P_{\Delta\omega}(z)$ simulated for the GaAs/AlAs coupled multilayer cavity. Reddish and bluish colors indicate the positive and negative signs of $P_{\Delta\omega}(z)$, respectively. The excitation source was a 100 fs Gaussian pulse incident from the left side.

where $P_{\Delta\omega}(z)$ is the Fourier component of $P(z,t)$, which is given by

$$P_{\Delta\omega}(z) = \sum_{\Omega} \chi^{(2)}(z,\omega,\omega') f_g(\omega) f_g(\omega') A^*(z,\omega) A(z,\omega') e^{-i\phi(z,\omega)} e^{i\phi(z,\omega')}. \quad (5)$$

Fig. 1 shows a position-dependent spectral map of $P_{\Delta\omega}(z)$ simulated under 100 fs Gaussian pulse irradiation from the left side. The simulated structure consists of two $\lambda/2$ layers (222 nm thick GaAs) coupled by a 10.5-period GaAs/AlAs (111 nm/130 nm) DBR, which is sandwiched between two 13-period DBRs. Linear refractive indices of 3.38 and 2.89 were used for GaAs and AlAs, respectively. The central wavelength of the 100 fs Gaussian pulse was set at the midpoint of the two cavity modes ($\lambda = 1491.6$ and 1516.2 nm), and the pulse had a spectral width (FWHM) of 33.3 nm, which corresponds to the bandwidth of 4.4 THz. In this case, the two cavity modes were simultaneously excited by a single 100 fs Gaussian pulse because the spectral width (33.3 nm) was wider than the mode wavelength difference (24.6 nm). For simplicity, $\chi^{(2)}(z,\omega,\omega')$ was assumed to be unity over the entire region. In Fig. 1, great enhancement of $P_{\Delta\omega}(z)$ can be observed in both cavity regions around a frequency of 3.3 THz, which corresponds to the optical frequency difference of the two cavity modes. This results from the product of the enhanced electric fields of the two modes due to the cavity effect [13]. Note that the sign of $P_{\Delta\omega}(z)$ around 3.3 THz is positive in the cavity region near the light incident surface, while the sign is negative on the other side of the cavity region. As discussed in the next section, the opposite signs of $P_{\Delta\omega}(z)$ in the two cavity regions are unfavorable to obtain the strong output terahertz signal because it leads to the significant cancellation of the radiated terahertz waves. An enhancement of $P_{\Delta\omega}(z)$ in both cavity regions is also evident around the zero frequency because each mode has a finite spectral width. However, the components around the zero frequency contribute a negligible amount to the electromagnetic field radiation. In addition to the cavity-mode related components, second-order polarization with a broad Fourier spectrum is generated in the vicinity of the light incident surface. The spectral shape is almost that given by the autocorrelation function of $f_g(\omega)$ used for the excitation pulse.

We now proceed to describe the temporal terahertz waveform generated by the second-order nonlinear polarization shown in Fig. 1. When the nonlinear polarization acts as a source of electromagnetic radiation, the radiated electric field is proportional to the second derivative of the polarization with respect to time. The electric field radiated by the local polarization element at position z should be summed over the entire structure taking into account of the z-dependent phase

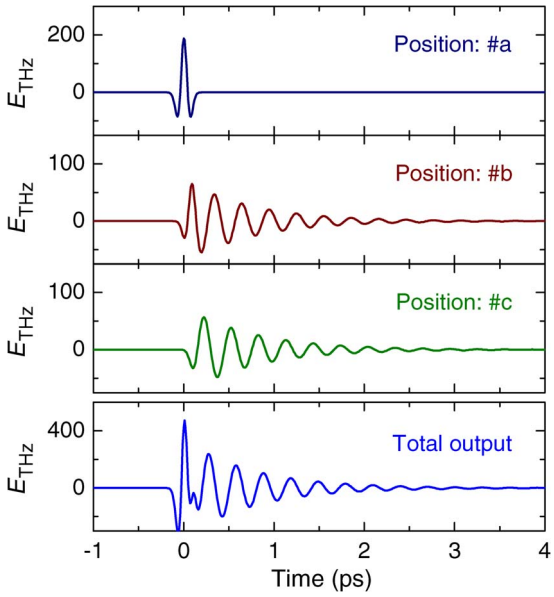

Fig. 2. Simulated temporal terahertz waveforms generated by polarization elements at the #a, #b, and #c positions indicated in Fig. 1. The output waveform is shown in the bottom panel.

factor to obtain the output electric field at the end of the structure. Here, it is assumed that the refractive index n_{THz} in the terahertz region is independent of z because the optical thickness of each layer is much smaller than the wavelength of the radiated field. The temporal terahertz waveform $E_{THz}(t)$ is thereby described by the relation

$$E_{THz}(t) \propto \sum_{z} \frac{\partial^2 P(z,t)}{\partial t^2} e^{ikz}, \tag{6}$$

where k is the wavenumber of the radiated electric field. Using (4) and $k = n_{THz}\Delta\omega/c$, (6) becomes

$$E_{THz}(t) \propto -\sum_{z}\sum_{\Delta\omega} \Delta\omega^2 P_{\Delta\omega}(z) e^{-i\Delta\omega(t-n_{THz}z/c)}, \tag{7}$$

where c is the speed of light in a vacuum.

Fig. 2 shows simulated temporal terahertz waveforms generated by the local polarization elements at the light incident surface (position #a indicated in Fig. 1) and the two cavity layers (#b and #c). Each temporal profile is plotted, taking into account the z-dependent phase shift given by $n_{THz}z/c$ in (7), where n_{THz} is assumed to be 3.65, which corresponds to the refractive index of GaAs around 2 THz [12]. The output waveform given by the summation of each radiated field is shown in the bottom panel of Fig. 2. At the light incident surface, the field radiation is limited to an extremely short period. The temporal profile is almost that given by the second derivative of the incident pulse shape with respect to time. On the other hand, decaying oscillations are clearly observed in both temporal profiles simulated for the cavity layer positions of #b and #c due to the enhanced DFG of the two cavity modes. The oscillation period corresponds to a mode frequency difference of 3.3 THz, and the decay constant is related to the spectral width of the two modes. Comparison of the two oscillations observed at #b and #c indicates a phase mismatch of almost half a period. The phase mismatch originates from the opposite sign of the enhanced $P_{\Delta\omega}(z)$ around the mode frequency difference, as shown in Fig. 1. The distance between the two cavity layers is not sufficient to compensate the phase mismatch; therefore, the radiated fields largely cancel each other out. However, in the output waveform, the oscillation behavior is still observed after the initial ultrafast response caused by the radiation near the light incident surface. If we introduce inversion of the

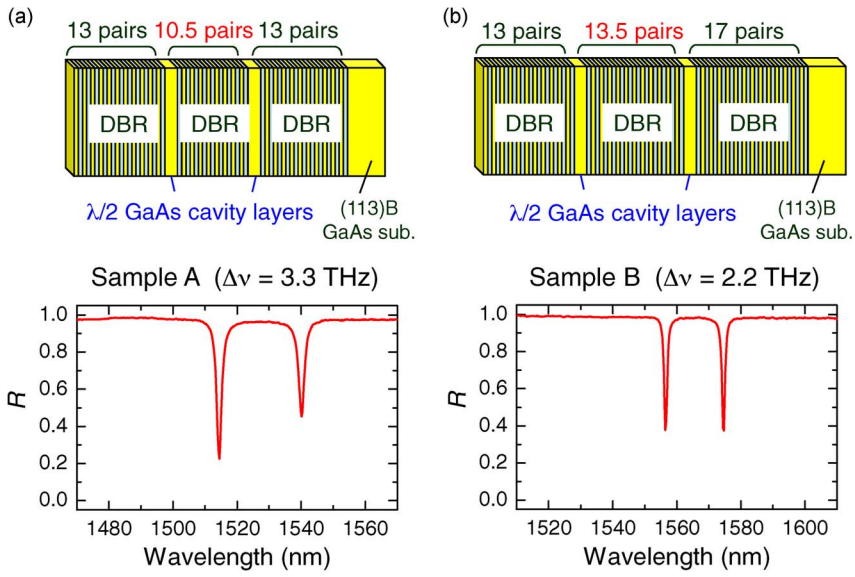

Fig. 3. Sample structures used in the experiments. Measured optical reflection spectra are given in the bottom panel. Two cavity modes with an optical frequency difference of (a) 3.3 and (b) 2.2 THz were observed in each spectrum.

nonlinear susceptibility at the middle of the coupling DBR, then the oscillation amplitude should be significantly enhanced in the output waveform. This situation can be accomplished by face-to-face bonding of two halves of the coupled cavity structure grown on the same high-index substrate [21]. The quantitative effect of the susceptibility inversion is dependent on the number of multilayer periods in the coupling DBR because it defines the mode frequency difference as well as the physical distance between the two cavity layers. Considering the Fourier spectra simulated for the present coupled cavity structures with and without the susceptibility inversion, an enhancement factor of 7 is estimated for the DFG signal at the mode frequency difference of 3.3 THz. A detailed discussion regarding the susceptibility inversion using the face-to-face bonding of two epitaxial wafers will be published elsewhere.

3. Comparison With Experiments

The two samples shown in Fig. 3 were prepared for experimental measurements. Both coupled cavity structures consisting of two $\lambda/2$ layers (222 nm thick GaAs) and three GaAs/AlAs (111 nm/130 nm) DBR multilayers were grown on (113)B-oriented GaAs substrates using solid-source molecular beam epitaxy (MBE). The detailed MBE growth procedures have been previously described in [16]. Sample A has the same structure as described in the previous section, while sample B has an increased number of multilayer periods in the coupling DBR. Using the 13.5-period GaAs/AlAs coupling DBR multilayer instead of the 10.5-period multilayer reduced the frequency difference of the two cavity modes from 3.3 to 2.2 THz, as shown in the measured optical reflection spectra of Fig. 3. The number of multilayer periods in the substrate-side DBR was also increased from 13 to 17 to improve the injection of two cavity-mode light for optical measurements. However, no significant improvement in the reflection dips of the two cavity modes of sample B was observed, due to the structural inhomogeneity.

Time-resolved terahertz waveform measurements were performed at room temperature using laser pulses with a pulse duration of $\sim$100 fs [19], [20]. Pump pulses of $\sim$1.5 μm that covered the two cavity modes were produced using an optical parametric oscillator (Spectra Physics Inc., Opal) pumped by a Ti:sapphire laser (Spectra Physics Inc., Tsunami) with an output wavelength of $\sim$0.81 μm and a repetition rate of 80 MHz. The measured spectrum of the pump pulses showed a spectral width (FWHM) of 25 nm, which corresponds to the bandwidth of 3.2 THz. The pump beam

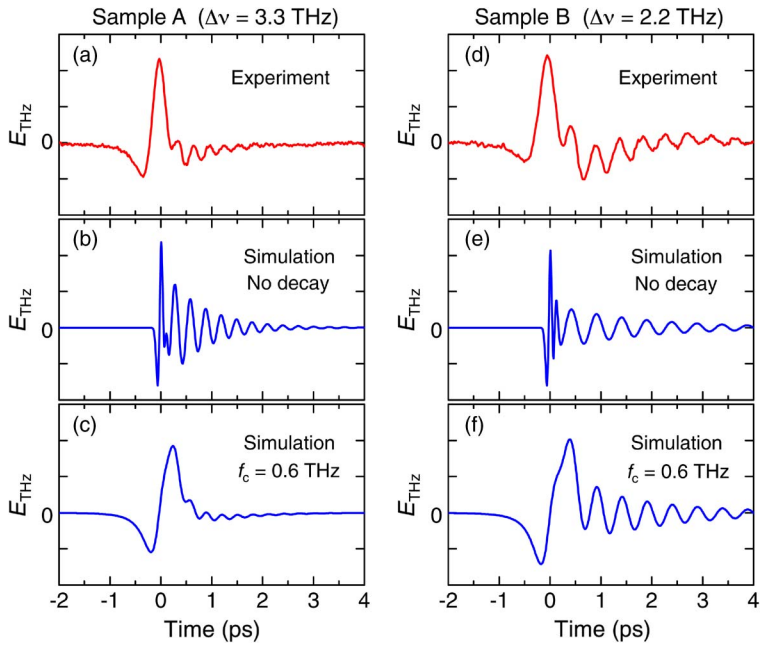

Fig. 4. (a, d) Measured temporal terahertz waveforms and (b, e) simulated waveforms for samples A and B. (c, f) Simulated waveforms assuming exponential decay of the signal sensitivity in the high frequency region.

(150 mW) was focused on the sample surface to a diameter of ~100 μm. The terahertz signal emitted from the substrate-side was detected using a dipole-type PC antenna with a gap of 6 μm, which was optically gated using a weak optical pulse beam (10 mW) from the Ti:sapphire laser. A commercially available PC antenna was used in this study. The PC antenna device acts as a terahertz receiver in the frequency range of about 1–4 THz. However, the frequency dependence of the signal sensitivity was not well calibrated. The pump pulses were polarized in the $[33\bar{2}]$ direction, and the polarization direction of the detected signal (which was parallel to the PC gap) was also aligned in the same $[33\bar{2}]$ direction. The time delay between the pump and gate pulses was controlled with a mechanical stage. A Si hemispherical lens was placed just behind the sample, and a Ge filter was used to prevent strong pump pulses from irradiating the PC antenna. Measurements were performed under a nitrogen atmosphere to prevent the absorption of terahertz waves by water vapor.

The measured temporal terahertz waveforms of samples A and B are shown in Fig. 4(a) and (b), respectively. The decaying oscillations due to the DFG of the two modes were clearly observed in both experimentally measured waveforms. However, the oscillation amplitudes were smaller than those obtained in the simulated waveforms shown in Fig. 4(b) and (e). This feature was more significant for sample A, for which the mode frequency difference (3.3 THz) was higher than that of sample B (2.2 THz). In addition, the broadened initial responses were observed compared with the simulated profiles. Power spectra given by Fourier transforms of the temporal waveforms measured for samples A and B are shown in Fig. 5(a) and (d), respectively. The corresponding simulated spectra are shown in Fig. 5(b) and (e), respectively. The discrepancies between the experimentally measured and simulated waveforms originated from the weaker signal intensities at higher frequencies of the experimentally measured waveforms. Therefore, the signal sensitivity of the PC antenna used for terahertz wave detection degrades in the higher frequency region. To take into account the frequency f dependence, exponential decay of signal sensitivity $S(f)$ is assumed and is represented as

$$S(f) = \exp\left(-\frac{f}{f_c}\right), \tag{8}$$

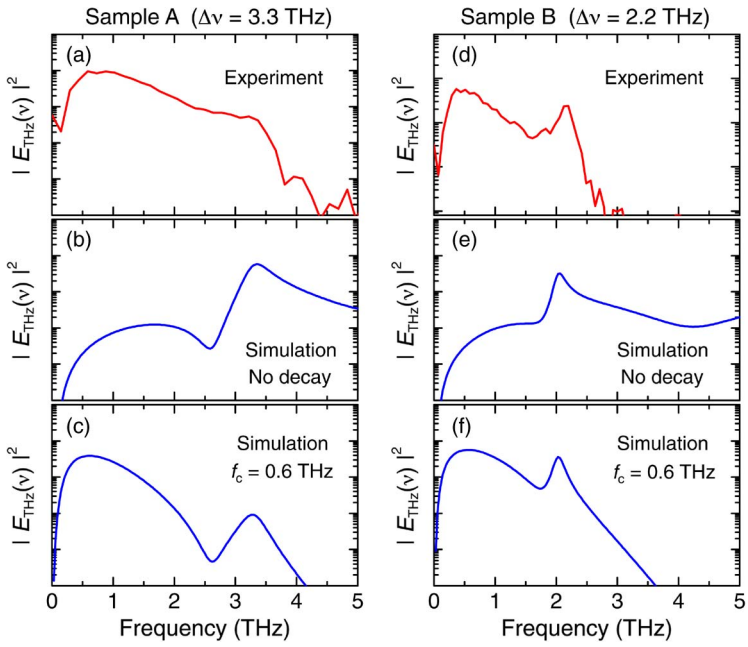

Fig. 5. Respective power spectra obtained by Fourier transforms of Fig. 4(a)–(f).

where f_c is the decay constant and gives the frequency response performance of the PC antenna device. The simulated waveforms of samples A and B using $f_c = 0.6$ THz are shown in Fig. 4(c) and (f), respectively. The broadened initial response and decreased oscillation amplitude observed in each experimentally measured waveform were well reproduced when we assume $f_c = 0.6$ THz in the simple exponential decay function of the signal sensitivity although the actual response function is considered to be more complicated. The simulated power spectra of samples A and B [Fig. 5(c) and (f), respectively] were also consistent with the experimental spectra shown in Fig. 5(a) and (d), respectively. Note that the simple model used in this study allows us to estimate terahertz emission properties from the coupled multilayer cavity, which is very useful to design the device structure for efficient terahertz emission using DFG of two cavity modes. For example, we can quantitatively evaluate effects of the polarization control for the intense terahertz emission induced by several fabrication techniques such as direct wafer-bonding. The consideration of other factors related to the structural inhomogeneity would be helpful for further understanding of terahertz wave generation from coupled cavity structures.

4. Conclusion

Temporal terahertz waveforms generated from GaAs/AlAs coupled multilayer cavity structures were studied using numerical simulation. The second-order nonlinear polarization induced by a 100 fs Gaussian pulse was calculated for terahertz DFG of the two cavity modes. In the calculation, the transfer matrix method was used to determine the internal electric field distributions of the injected frequency components. Then, the Fourier component map of the nonlinear polarization dependence on the frequency and spatial position was used to deduce the output temporal waveform by summation of the electric fields radiated by the local polarization elements. In the simulated waveform, the decaying oscillation due to efficient DFG of the two cavity modes was observed after the initial ultrafast response near the incident surfaces. The simulated and experimental results were compared for two different samples of GaAs/AlAs coupled multilayer cavity structures grown on (113)B GaAs substrates by MBE. The broadened initial responses and weak oscillation amplitudes of the experimentally measured waveforms were explained by

assuming an exponential decay of the signal sensitivity in the high frequency region. These results are very useful for the design of novel terahertz emission devices based on coupled multilayer cavity structures.

References

[1] R. Köhler, A. Tredicucci, F. Beltram, H. E. Beere, E. H. Linfield, A. G. Davies, D. A. Ritchie, R. C. Iotti, and F. Rossi, "Terahertz semiconductor-heterostructure laser," *Nature*, vol. 417, no. 6885, pp. 156–159, May 2002.

[2] B. S. Williams, "Terahertz quantum-cascade lasers," *Nature Photon.*, vol. 1, no. 9, pp. 517–525, Sep. 2007.

[3] M. A. Belkin, J. A. Fan, S. Hormoz, F. Capasso, S. P. Khanna, M. Lachab, A. G. Davies, and E. H. Linfield, "Terahertz quantum cascade lasers with copper metal-metal waveguides operating up to 178 K," *Opt. Exp.*, vol. 16, no. 5, pp. 3242–3248, Mar. 2008.

[4] M. Asada, S. Suzuki, and N. Kishimoto, "Resonant tunneling diodes for sub-terahertz and terahertz oscillators," *Jpn. J. Appl. Phys.*, vol. 47, no. 6, pp. 4375–4384, Jun. 2008.

[5] S. Matsuura, M. Tani, and K. Sakai, "Generation of coherent terahertz radiation by photomixing in dipole photoconductive antennas," *Appl. Phys. Lett.*, vol. 70, no. 5, pp. 559–561, Feb. 1997.

[6] H. Ito, F. Nakajima, T. Furuta, K. Yoshino, and T. Ishibashi, "Photonic terahertz-wave generation using antenna-integrated uni-travelling-carrier photodiode," *Electron. Lett.*, vol. 39, no. 25, pp. 1828–1829, Dec. 2003.

[7] T. Tanabe, K. Suto, J. Nishizawa, K. Saito, and T. Kimura, "Tunable terahertz wave generation in the 3- to 7-THz region from GaP," *Appl. Phys. Lett.*, vol. 83, no. 2, pp. 237–239, Jul. 2003.

[8] T. Taniuchi and H. Nakanishi, "Collinear phase-matched terahertz-wave generation in GaP crystal using a dual-wavelength optical parametric oscillator," *J. Appl. Phys.*, vol. 95, no. 12, pp. 7588–7591, Jun. 2004.

[9] I. Tomita, H. Suzuki, H. Ito, H. Takenouchi, K. Ajito, R. Rungsawang, and Y. Ueno, "Terahertz-wave generation from quasi-phase-matched GaP for 1.55μm pumping," *Appl. Phys. Lett.*, vol. 88, no. 7, pp. 071118-1–071118-3, Feb. 2006.

[10] D. H. Auston, K. P. Cheung, and P. R. Smith, "Picosecond photoconducting Hertzian dipoles," *Appl. Phys. Lett.*, vol. 45, no. 3, pp. 284–286, Aug. 1984.

[11] P. Y. Han and X.-C. Zhang, "Coherent, broadband midinfrared terahertz beam sensors," *Appl. Phys. Lett.*, vol. 73, no. 21, pp. 3049–3051, Nov. 1998.

[12] M. Nagai, K. Tanaka, H. Ohtake, T. Bessho, T. Sugiura, T. Hirosumi, and M. Yoshida, "Generation and detection of terahertz radiation by electro-optical process in GaAs using 1.56μm fiber laser pulses," *Appl. Phys. Lett.*, vol. 85, no. 18, pp. 3974–3976, Nov. 2004.

[13] T. Kitada, F. Tanaka, T. Takahashi, K. Morita, and T. Isu, "GaAs/AlAs coupled multilayer cavity structures for terahertz emission devices," *Appl. Phys. Lett.*, vol. 95, no. 11, pp. 111106-1–111106-3, Sep. 2009.

[14] N. Yamada, Y. Ichimura, S. Nakagawa, Y. Kaneko, T. Takeuchi, and N. Mikoshiba, "Second-harmonic generation in vertical-cavity surface-emitting laser," *Jpn. J. Appl. Phys.*, vol. 35, no. 5A, pp. 2659–2664, May 1996.

[15] Y. Kaneko, S. Nakagawa, Y. Ichimura, and N. Yamda, "Blue vertical-cavity surface-emitting lasers on second-harmonic generation grown on (311)B and (411)A GaAs substrates," *J. Appl. Phys.*, vol. 87, no. 4, pp. 1597–1603, Feb. 2000.

[16] F. Tanaka, T. Takahashi, K. Morita, T. Kitada, and T. Isu, "Strong sum frequency generation in a GaAs/AlAs coupled multilayer cavity grown on a (113)B-oriented GaAs substrate," *Jpn. J. Appl. Phys.*, vol. 49, no. 4, pp. 04DG01-1–04DG01-3, Apr. 2010.

[17] K. Morita, F. Tanaka, T. Takahashi, T. Kitada, and T. Isu, "Optical anisotropy of strongly enhanced sum frequency generation in (113)B GaAs/AlAs coupled multilayer cavity," *Appl. Phys. Exp.*, vol. 3, no. 7, pp. 072801-1–072801-3, Jul. 2010.

[18] F. Tanaka, T. Takimoto, K. Morita, T. Kitada, and T. Isu, "Time-resolved measurements of sum-frequency generation strongly enhanced in (113)B GaAs/AlAs coupled multilayer cavity," *Jpn. J. Appl. Phys.*, vol. 50, no. 4, pp. 04DG03-1–04DG03-4, Apr. 2011.

[19] K. Morita, S. Katoh, T. Takimoto, F. Tanaka, Y. Nakagawa, S. Saito, T. Kitada, and T. Isu, "Generation of terahertz radiation from two cavity modes of a GaAs/AlAs coupled multilayer cavity," *Appl. Phys. Exp.*, vol. 4, no. 10, pp. 102102-1–102102-3, Oct. 2011.

[20] S. Katoh, T. Takimoto, Y. Nakagawa, K. Morita, T. Kitada, and T. Isu, "Terahertz radiation from a (113)B GaAs/AlAs coupled multilayer cavity generated by ultrashort laser pulse excitation," *Jpn. J. Appl. Phys.*, vol. 51, no. 4, pp. 04DG05-1–04DG05-4, Apr. 2012.

[21] T. Kitada, F. Tanaka, T. Takahashi, K. Morita, and T. Isu, "Novel terahertz emission devices based on efficient optical frequency conversion in GaAs/AlAs coupled multilayer cavity structures on high-index substrates," in *Proc. SPIE*, Feb. 2011, vol. 7937, pp. 79371H-1–79371H-6.